Electrochemical and Solid-State Letters, **14** (2) H88-H92 (2011)
1099-0062/2010/14(2)/H88/5/$28.00 © The Electrochemical Society

Enhancement of a-IZO TTFT Performance by Using Y_2O_3/Al_2O_3 Bilayer Dielectrics

Ai Hua Chen, Ling Yan Liang, Hai Zhong Zhang, Zhi Min Liu, Xiao Juan Ye, Zheng Yu, and Hong Tao Cao[z]

Ningbo Institute of Materials Technology and Engineering, Chinese Academy of Sciences, Ningbo 315201, People's Republic of China

A comparison study was performed on radio frequency sputtered amorphous In–Zn–O transparent thin-film transistors (a-IZO TTFTs) using Y_2O_3 and Y_2O_3/Al_2O_3 dielectrics. Y_2O_3 has strong affinity for water and carbon dioxide molecules present in the air, which would induce a great deal of Y–O• electron traps at the Y_2O_3/a-IZO interface and ruin the device performance eventually. It is proposed that an Al_2O_3 capping layer is utilized to avoid chemical reaction on the surface of Y_2O_3, then the detrimental effects that yield electron trap states are circumvented.
© 2010 The Electrochemical Society. [DOI: 10.1149/1.3519412] All rights reserved.

Manuscript submitted August 26, 2010; revised manuscript received November 1, 2010. Published December 2, 2010.

Recently, oxide semiconductor-based transparent thin-film transistors (TTFTs) have been explored intensively for their higher mobility compared to amorphous silicon or organic counterpart.[1-3] Among the oxide-based TTFTs, amorphous In–Zn–O (a-IZO) used as the channel has attracted considerable attention, as it could be fabricated at low temperature and still maintained good performance.[4,5] Besides, the carrier mobility and conductivity of the a-IZO films could be tuned by controlling either the composition or the deposition atmosphere.[6-8] So a-IZO is regarded as one of the multifunctional materials that can be utilized not only as active layers but also as the source/drain electrodes, which allows one material with tunable properties to be used in one device.

Also, it is very crucial to choose a well-matched dielectric to gate the semiconductor layer of a-IZO. Y_2O_3 is one of the promising candidates, due to its high dielectric constant (~ 15), wide bandgap (~ 5.5 eV), and high breakdown voltage.[9-12] Moreover, Y_2O_3 used as the gate insulator exhibits low leakage current that is beneficial to lower power consumption.[13] In this work, we fabricated TTFTs using a-IZO and Y_2O_3 as the active layer and gate insulator, respectively (marked as Y_2O_3/a-IZO TTFT). However, it is found that Y_2O_3 has a strong affinity for water and carbon dioxide molecules in the air and hydroxyl and carbonyl groups present at the Y_2O_3 surface,[14] which would degrade the Y_2O_3/a-IZO interface quality and ruin the device performance inevitably. In order to circumvent the situation, it is proposed that Y_2O_3/Al_2O_3 bilayer dielectrics (marked as Y_2O_3/Al_2O_3/a-IZO TTFT) are utilized to eliminate the fatal contribution arising from hydroxyl and carbonyl groups, because Al_2O_3 is known as a high-k (~ 9) dielectric material with a wide bandgap (~ 8.8) and high chemical stability.[15] A comparison study of the electrical properties of both the devices is addressed in this article.

Experimental

The a-IZO TTFTs with a bottom gate structure were fabricated on the indium tin oxide (ITO) glass substrates that served as the gate electrode (resistivity $\rho < 0.01\ \Omega$ cm). The ITO glass was ultrasonically cleaned with acetone (5 min), ethanol (5 min), and deionized water (5 min) sequentially for two times. 300 nm Y_2O_3 film and 250 nm Y_2O_3/50 nm Al_2O_3 double layers were deposited on ITO glass by reactive rf magnetron (ULVAC, Japan, Jsputter 8000) at room temperature. After that, the samples had intentionally been exposed to air for ten days to highlight the effects coming from the chemical functional groups present on the dielectric surface. Then the a-IZO channel layer and source/drain electrodes, which are patterned by the first and second shadow masks, respectively, were prepared by rf magnetron cosputtering, applying a ZnO target and an In_2O_3 target. The deposition parameters of all the layers were listed in Table I. The a-IZO channel was defined with a width (W) of 500 μm and a length (L) of 100 μm. The capacitance of the dielectrics was evaluated using a metal–insulator–metal (MIM) structure, in which the ITO glass was used as the bottom electrode and substrate, while the copper thin film (200 nm) was deposited by electron beam evaporation (ULVAC MUE-ECO-EB) used as the top electrode.

The thickness of all films was determined ex situ using spectroscopic ellipsometer (J. A. Woollam Co., Inc., USA, M-2000DI). The surface morphologies of the dielectric films were examined via the atomic force microscope (AFM; Veeco Dimention V, USA). The chemical states of the Y_2O_3 film were checked using transmission Fourier transform infrared (FTIR) spectroscopy (Nicolet 6700) in the range of 4000–400 cm^{-1}. The surface chemical states of Y_2O_3 and Al_2O_3 films were further analyzed by the X-ray photoelectron spectroscopy (XPS, Kratos Analytical Ltd., U.K.). The electrical characteristics of the MIM capacitors and TTFTs were measured with a precision semiconductor analyzer (Keithley 4200, USA) in the dark at room temperature. The stoichiometry and microstructure of a-IZO films could be found elsewhere.[16]

Results and Discussion

The surface morphologies of the single Y_2O_3 layer and Y_2O_3/Al_2O_3 double layer were examined by the AFM, as shown in Fig. 1. It is found that the root-mean-square roughness of single Y_2O_3 dielectric (6.71 nm) approximates to that of the bilayer (7.11 nm). The rough surface of the Y_2O_3 film is due to the rough ITO substrate (roughness ~ 3.5 nm) and the polycrystalline nature of the Y_2O_3 film.[17] As for the bilayer, however, the rough starting Y_2O_3 film might promote the shadowing effect and self-enhanced roughening of the upper Al_2O_3 film.[18]

As shown in Fig. 2, the bands approximately located at 563 and 470 cm^{-1} are assigned to the Y–O vibration of cubic Y_2O_3,[19] indicating the crystalline nature of the film. It is noted that the bands approximately at 3475 and 1620 cm^{-1} are due to the OH bonding and the bands present at 1510 and 1410 cm^{-1} correspond to C=O asymmetric stretching vibration,[14,19] suggesting the existence of water and CO_2 adsorbed in the Y_2O_3 film.

Figures 3a and b show the Y 3d and O 1s XPS spectra of the Y_2O_3 film, respectively. The binding energy peak positions centered at 156.49 and 158.54 eV are assigned to Y_2O_3, while those at 158.21 and 160.06 eV are allocated to $Y(OH)_3$.[20] The molar ratio of Y_2O_3 and $Y(OH)_3$ is 1.38, which indicates that exposing Y_2O_3 in air can lead to significant hydroxide adsorption as the above FTIR analysis, and the –OH functional groups are able to react with Y_2O_3 to generate $Y(OH)_3$.[14] Furthermore, the Y_2O_3 film could also adsorb some CO_2 to yield $Y_2(CO_3)_3$,[20] as shown in Fig. 3b. Figures 3c and d display the Al 2p and O 1s XPS spectra on the surface of

[z] E-mail: h_cao@nimte.ac.cn

Downloaded 02 Dec 2010 to 130.237.29.138. Redistribution subject to ECS license or copyright; see http://www.ecsdl.org/terms_use.jsp

Table I. Main deposition parameters of Y_2O_3, Al_2O_3, and a-IZO films.

Films	Y_2O_3	Al_2O_3	a-IZO channels		a-IZO electrodes	
Targets	Y	Al	ZnO	In_2O_3	ZnO	In_2O_3
Sputtering power (W)	80	80	100	70	100	70
Working pressure (Pa)	0.47	0.48	0.46		0.46	
O_2:Ar (sccm)	0.5:10	0.6:10	2:8		0:10	
Film thickness (nm)	300/250	0/50	114		220	
Substrate temperature	Room temperature					
Base pressure (Pa)	9.0×10^{-5}					

overlying Al_2O_3 film in the Al_2O_3/Y_2O_3 bilayer. It is observed that the signal coming from the physisorbed H_2O molecule is distinguishable, but there is just one Al 2p peak allocated to Al_2O_3 (74.4–75.8 eV in Ref. 21), precluding the existence of $Al(OH)_3$ (73.9–74.4 eV in Ref. 22). In comparison with the physisorption characteristic of the Al_2O_3 surface, the chemically reacted surface of Y_2O_3 is less resistant against the sputtering-process-induced damage and would affect the electrical properties significantly, which will be discussed next in more details.

Figures 4a and b display the output characteristics of the Y_2O_3/a-IZO TTFT and Y_2O_3/Al_2O_3/a-IZO TTFT, respectively. Both devices show typical transistor characteristics with clear pinch-off voltage, high on-current, and hard saturation at a low drain–source voltage ($V_{DS} \sim 2$ V). It is observed herein that there is an oversaturation hump of the drain–source current (I_{DS}) of the Y_2O_3/a-IZO TTFT in Fig. 4a, which implies that the transporting electrons modulated by the gate voltage are trapped by the acceptor states at the Y_2O_3/a-IZO interface, resulting in insufficient channel carrier charges.[23] However, when the bilayer of dielectrics is applied instead of the single Y_2O_3 layer, the complete vanishment of the so-called oversaturation hump of the output curve was observed (Fig. 4b), which will be further discussed in the following section.

The transfer curves of the studied devices are depicted in Fig. 5. The field-effect mobility (μ_{FE}) in the saturation region and subthreshold swing (S) were estimated using the following relations: $\mu_{FE} = 2LI_{DS}/WC_i(V_{GS} - V_{th})^2$, and $S = dV_{GS}/d(\log I_{DS})$, where C_i, V_{GS}, and V_{th} are the gate insulator capacitance, gate–source voltage, and threshold voltage, respectively. The inset of Fig. 5 shows the capacitances of the Cu/Y_2O_3/ITO and $Cu/Al_2O_3/Y_2O_3$/ITO structures measured at 1 MHz. The capacitance of the $Cu/Al_2O_3/Y_2O_3$/ITO capacitor (38.8 nF/cm^2) is a little smaller than that of the Cu/Y_2O_3/ITO structure (39.9 nF/cm^2), which is caused by the lower dielectric constant of Al_2O_3 ($\sim$ 9) compared to Y_2O_3 ($\sim$15).

The electrical parameters of both the TTFTs are listed in Table II. The Y_2O_3/Al_2O_3/a-IZO TTFT demonstrates a better on/off ratio, a higher μ_{FE}, and a smaller S than those of Y_2O_3/a-IZO TTFT. In particular, the device parameters of the Y_2O_3/Al_2O_3/a-IZO TTFT include a subthreshold swing (S) of 72.7 meV/decade, a threshold voltage (V_{th}) of 1.9 V, and a field effect mobility (μ_{FE}) of 238 cm^2 V^{-1} s^{-1} (at 1 MHz). The on and off currents are 3×10^{-4} and 1×10^{-11} A, respectively, giving an on/off current ratio of about 3×10^7. Considering our device geometry and the fringing electric field effect,[24,25] the corrected μ_{FE} is about 95.4 cm^2 V^{-1} s^{-1}. Even though the corrected saturation field effect mobility in this study is definitely overestimated (without considering the contribution from the capacitance dispersion), these electrical properties are comparable to the reported values.[26,27]

The subthreshold swing (S) is one of the crucial parameters of the device, which is in effect a measure of the rate at which a device "turns on."[28] The S value is an indicant of the bulk trap density (N_{bs})

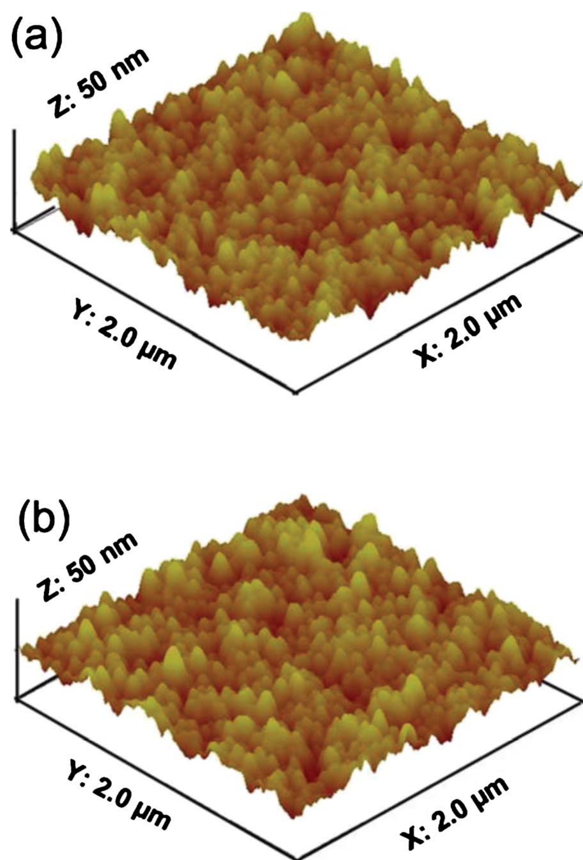

Figure 1. (Color online) The AFM images of (a) the Y_2O_3 single-layer and (b) the Y_2O_3/Al_2O_3 double-layer dielectrics.

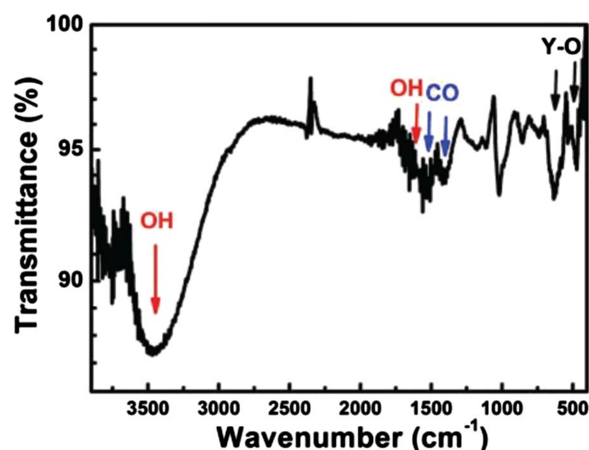

Figure 2. (Color online) The FTIR spectra of the Y_2O_3 films.

Downloaded 02 Dec 2010 to 130.237.29.138. Redistribution subject to ECS license or copyright; see http://www.ecsdl.org/terms_use.jsp

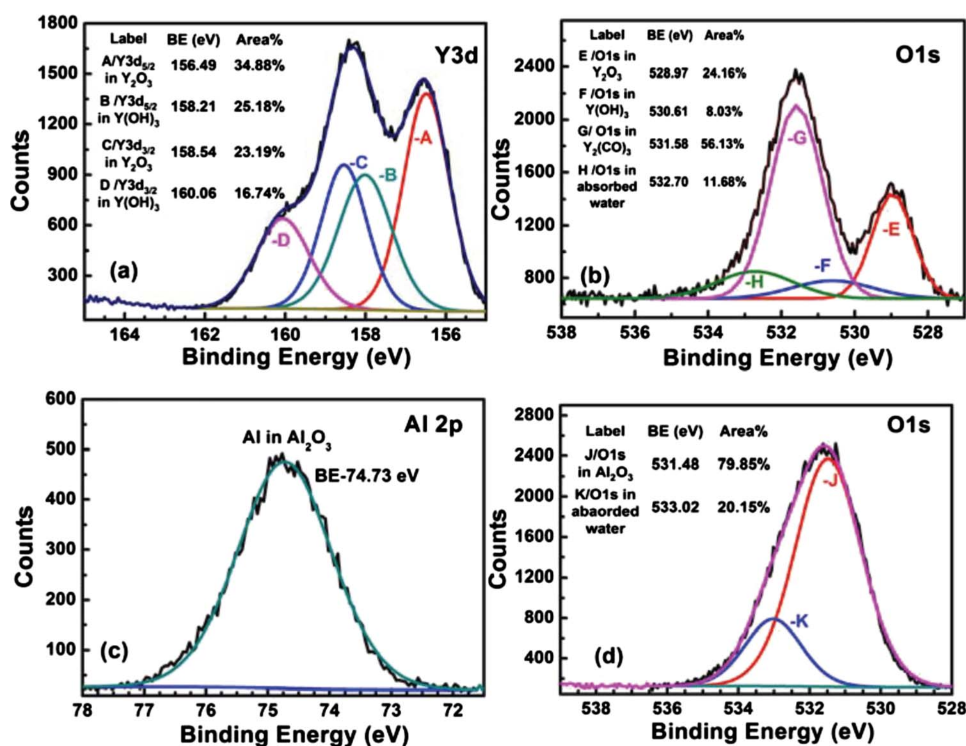

Figure 3. (Color online) The XPS spectra of Y_2O_3 and Al_2O_3 films: (a) Y 3d and (b) O 1s spectra of the Y_2O_3 surface; (c) Al 2p and (d) O 1s spectra of the Al_2O_3 capped on the Y_2O_3.

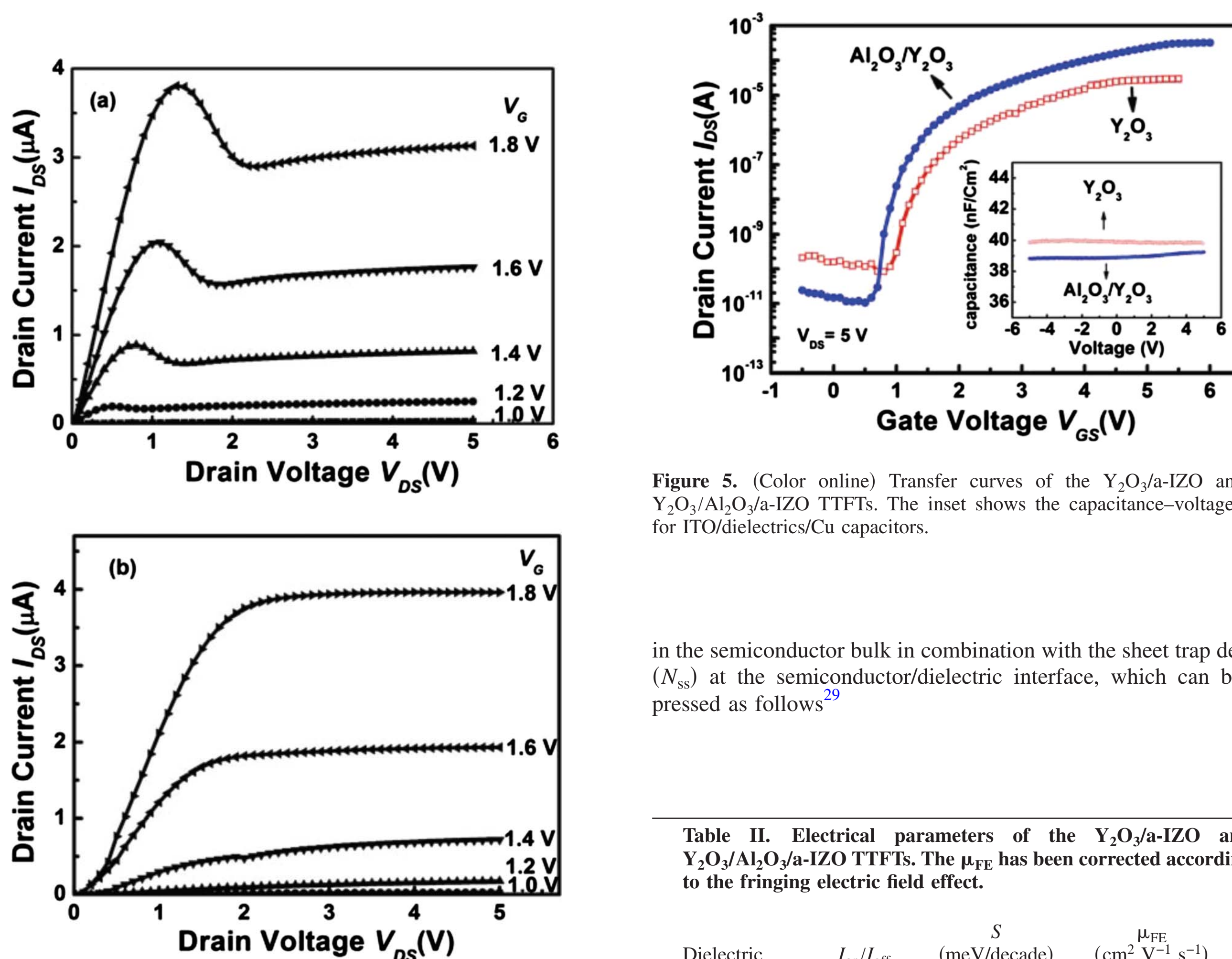

Figure 4. Output curves of (a) the Y_2O_3/a-IZO TTFT and (b) the Y_2O_3/Al_2O_3/a-IZO TTFT.

Figure 5. (Color online) Transfer curves of the Y_2O_3/a-IZO and the Y_2O_3/Al_2O_3/a-IZO TTFTs. The inset shows the capacitance–voltage plots for ITO/dielectrics/Cu capacitors.

in the semiconductor bulk in combination with the sheet trap density (N_{ss}) at the semiconductor/dielectric interface, which can be expressed as follows[29]

Table II. Electrical parameters of the Y_2O_3/a-IZO and Y_2O_3/Al_2O_3/a-IZO TTFTs. The μ_{FE} has been corrected according to the fringing electric field effect.

Dielectric	I_{on}/I_{off}	S (meV/decade)	μ_{FE} ($cm^2\ V^{-1}\ s^{-1}$)	V_{th} (V)
Y_2O_3	4×10^5	162	15.6	2.0
Al_2O_3/Y_2O_3	3×10^7	72.7	95.4	1.9

Downloaded 02 Dec 2010 to 130.237.29.138. Redistribution subject to ECS license or copyright; see http://www.ecsdl.org/terms_use.jsp

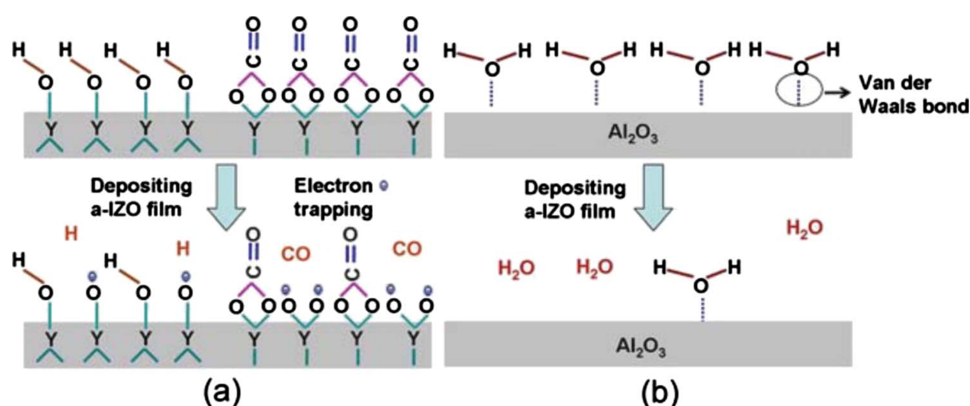

Figure 6. (Color online) Schematic diagram of functional group electron trapping on (a) the chemically reacted surface of Y_2O_3 and (b) the physisorption surface of Al_2O_3.

$$S = \frac{kT}{q\log(e)}\left[1 + \frac{q}{C_i}(\sqrt{\varepsilon_s N_{bs}} + qN_{ss})\right] \quad [1]$$

where ε_s, q, k, and T are the semiconductor dielectric constant, absolute value of the electron charge, Boltzmann constant, and temperature, respectively. Compared to the Y_2O_3/a-IZO TTFT, the S value of Y_2O_3/Al_2O_3/a-IZO TTFT is improved to be 72.7 meV/decade, which is close to the theoretical limit (60 meV/decade) for an ideal TFT at room temperature. However, it is necessary to clarify whether N_{bs} or N_{ss} is the main contributor to the reduction of the subthreshold swing. Because the deposition conditions for a-IZO films are identical, and the surface morphologies of the underlying dielectric surface to grow the overlying a-IZO are similar (see Fig. 1), the bulk trap densities in the semiconductor layer are believed to differ marginally from each other. Therefore, the improvement of the subthreshold swing for the Y_2O_3/Al_2O_3/a-IZO TTFT is thought to be stemmed exclusively from the reduction of N_{ss} rather than N_{bs}. The nature of interface traps is dependent on the intricate microstructural details of the interaction between the semiconductor and dielectric.[30] From the above mentioned XPS and FTIR results, exposing Y_2O_3 dielectrics for an extended period of time in air can promote the outermost surface of Y_2O_3 to react with H_2O and CO_2 in the air, producing $Y(OH)_3$ and $Y_2(CO_2)_3$, respectively. When the a-IZO overlayer was deposited on the Y_2O_3 dielectric by rf magnetron sputtering, the Y–O–H (Y–O–C═O) bonds at the Y_2O_3 surface might be relatively easily broken into Y–O• bond and H (Y–O• and CO) by some energetic In, Zn, and O particles (as shown in Fig. 6a), because the bonding energy of either –OH (424 kJ/mol) or –C═O (360 kJ/mol) bond is much smaller than that of the Y–O (685 kJ/mol) bond.[31] The electrons in the channel are easily captured by the Y–O• traps, analogous to the Si–O• traps in SiO_2 film.[32] In contrast, it is deduced that the Al_2O_3 layer could also adsorb some water; however, the adsorbed water definitely did not interact with the Al_2O_3 dielectric based on the Al 2p and O 1s XPS spectra. So it is inferred that the Van der Waal force keeps H_2O molecules linked to the Al_2O_3 surface with the nature of physical adsorption. When depositing the a-IZO channel layer, the "Van der Waal bond" between adsorbed H_2O molecule and Al_2O_3 would affirmatively be broken by the energetic In, Zn, and O particles, seldom yielding acceptor trap states at the Al_2O_3/a-IZO interface, as displayed in Fig. 6b. In a word, the acceptor trap states at the Y_2O_3/a-IZO interface are far more than those at the Al_2O_3/a-IZO interface, giving rise to a lager S as well as an oversaturation hump of the output curve for the former device.

The μ_{FE} of the device is determined by the semiconductor itself, which is influenced simultaneously by the carrier scattering caused by the roughness of the dielectric surface and the trap states at the semiconductor/dielectric interface. From the AFM images, it is found that the surface roughness of both the cases is so similar that the influence on the carrier transporting could be ignored. As discussed in the above paragraph, the N_{ss} at the Y_2O_3/a-IZO interface is far more than that at the Al_2O_3/a-IZO interface. As a result, the carriers are seriously trapped or/and detrapped in the Y_2O_3/a-IZO TTFT, which leads to a lower mobility in comparison with the Y_2O_3/Al_2O_3/a-IZO TTFT.

Conclusions

In this work, the electrical properties of a-IZO TTFTs based on Y_2O_3 single-layer and Al_2O_3/Y_2O_3 bilayer dielectrics were investigated comparatively. It is found that exposing Y_2O_3 dielectrics to the ambient air can yield $Y(OH)_3$ and $Y(CO_3)_2$ which might be easily broken during the subsequent sputtering of channel layers, inducing a poor dielectric/semiconductor interface with a large amount of Y–O• electron traps and finally deteriorating the TTFT performance. In comparison, however, a thin Al_2O_3 capping layer on the Y_2O_3 surface can effectively avoid the chemical reactions and hinder the generation of the electron traps, resultantly bringing about excellent electrical properties, i.e., no oversaturation hump, a large I_{on}/I_{off} ratio (3×10^7), and especially a very high μ_{FE} (95.4 cm^2 V^{-1} s^{-1}) and a very small S (72.7 meV/decade). The competitive device performance, together with room-temperature fabrication processes, proposes a hopeful application of the TTFT technology for the future transparent electronics.

Acknowledgments

A.H.C. and L.Y.L. contributed equally to this work. The authors are grateful for the financial support of the key project of the Natural Science Foundation of Zhejiang Province (grant no. Z4080347), the Qianjiang Talent Program of Zhejiang Province (grant no. 2009R10072), the CAS/SAFEA International Partnership Program for Creative Research Teams, the aided program for Science and Technology Innovative Research Team of Ningbo Municipality (2009B21005), and the Special Foundation of President of the Chinese Academy of Sciences (Grant no. 080421WA01).

References

1. R. L. Hoffman, B. J. Norris, and J. F. Wager, *Appl. Phys. Lett.*, **82**, 733 (2003).
2. P. F. Carcia, R. S. McLean, M. H. Reilly, and G. Nunes, *Appl. Phys. Lett.*, **82**, 1117 (2003).
3. H. Q. Chiang, J. F. Wager, R. L. Hoffman, J. Jeong, and D. A. Keszler, *Appl. Phys. Lett.*, **86**, 013503 (2005).
4. E. Fortunato, P. Barquinha, G. Gonçalves, L. Pereira, and R. Martins, *Solid-State Electron.*, **52**, 443 (2008).
5. J. I. Song, J. S. Park, H. Kim, Y. W. Heo, J. H. Lee, J. J. Kim, G. M. Kim, and B. D. Choi, *Appl. Phys. Lett.*, **90**, 022106 (2007).
6. M. G. McDowell and I. G. Hill, *IEEE Trans. Electron Devices*, **56**, 343 (2009).
7. B. Yaglioglu, H. Y. Yeom, and D. C. Paine, *Appl. Phys. Lett.*, **86**, 261908 (2005).
8. E. Fortunato, A. Pimentel, A. Gonçalves, A. Marques, and R. Martins, *Thin Solid Films*, **502**, 104 (2006).
9. M. Leskela, K. Kukli, and M. Ritala, *J. Alloys Compd.*, **418**, 27 (2006).
10. M. Leskela and M. Ritala, *J. Solid State Chem.*, **171**, 170 (2003).
11. D. A. Neumayer and E. Cartier, *J. Appl. Phys.*, **90**, 1801 (2001).
12. J. Hudner, H. Ohlsen, and E. Fredriksson, *Vacuum*, **46**, 967 (1995).
13. R. H. Horng, D. S. Wuu, J. W. Yu, and C. Y. Kung, *Thin Solid Films*, **289**, 234 (1996).

Downloaded 02 Dec 2010 to 130.237.29.138. Redistribution subject to ECS license or copyright; see http://www.ecsdl.org/terms_use.jsp

14. D. Niu, R. W. Ashcraft, and G. N. Parsons, *Appl. Phys. Lett.*, **80**, 3575 (2002).
15. M. L. Green, E. P. Gusev, R. Degraeve, and E. L. Garfunkel, *J. Appl. Phys.*, **90**, 2057 (2001).
16. A. H. Chen, H. T. Cao, H. Z. Zhang, L. Y. Liang, Z. M. Liu, Z. Yu, and Q. Wan, *Microelectron. Eng.*, **87**, 2019 (2010).
17. H. Z. Zhang, L. Y. Liang, A. H. Chen, Z. M. Liu, Z. Yu, H. T. Cao, and Q. Wan, *Appl. Phys. Lett.*, **97**, 122108 (2010).
18. M. Voigt, A. Bergmaier, G. Dollinger, and M. Sokolowski, *J. Vac. Sci. Technol. A*, **27**, 234 (2009).
19. H. Guo, W. Zhang, L. Lou, A. Brioude, and J. Mugnier, *Thin Solid Films*, **458**, 274 (2004).
20. S. A. Barve, Jagannath, N. Mithal, M. N. Deo, N. Chand, B. M. Bhanage, L. M. Gantayet, and D. S. Patil, *Surf. Coat. Technol.*, **204**, 3167 (2010).
21. C. S. Yang, J. S. Kim, J. W. Choi, M. H. Kwon, Y. J. Kim, J. G. Choi, and G. T. Kim, *J. Ind. Eng. Chem. (Seoul, Repub. Korea)*, **6**, 149 (2000).
22. J. T. Kloprogge, L. V. Duong, B. J. Wood, and R. L. Frost, *J. Colloid Interface Sci.*, **296**, 572 (2006).
23. M. S. Oh, K. Lee, J. H. Song, B. H. Lee, M. M. Sung, D. K. Hwang, and S. Im, *J. Electrochem. Soc.*, **155**, H1009 (2008).
24. K. Okamura, D. Nikolova, N. Mechau, and H. Hahn, *Appl. Phys. Lett.*, **94**, 183503 (2009).
25. L. Zhang, J. Li, X. W. Zhang, X. Y. Jiang, and Z. L. Zhang, *Appl. Phys. Lett.*, **95**, 072112 (2009).
26. J. S. Lee, S. Chang, S. M. Koo, and S. Y. Lee, *IEEE Electron Device Lett.*, **31**, 225 (2010).
27. N. C. Su, S. J. Wang, and A. Chin, *Electrochem. Solid-State Lett.*, **13**, H8 (2010).
28. R. B. M. Cross, M. M. De Souza, S. C. Deane, and N. D. Young, *IEEE Trans. Electron Devices*, **55**, 1109 (2008).
29. A. Rolland, J. Richard, J. P. Kleider, and D. Mencaraglia, *J. Electrochem. Soc.*, **140**, 3679 (1993).
30. M. H. Yoon, C. Kim, A. Facchetti, and T. J. Marks, *J. Am. Chem. Soc.*, **128**, 12851 (2006).
31. K. Miwa, N. Takada, and K. Sasaki, *J. Vac. Sci. Technol. A*, **27**, 831 (2009).
32. B. L. Yang, H. Wong, and Y. C. Cheng, *Chin. Phys. Lett.*, **12**, 420 (1995).

Downloaded 02 Dec 2010 to 130.237.29.138. Redistribution subject to ECS license or copyright; see http://www.ecsdl.org/terms_use.jsp